NANO LETTERS

Letter

pubs.acs.org/NanoLett

Site-Controlled VLS Growth of Planar Nanowires: Yield and Mechanism

Chen Zhang, Xin Miao, Parsian K. Mohseni, Wonsik Choi, and Xiuling Li*

Department of Electrical and Computer Engineering, Micro and Nanotechnology Laboratory, University of Illinois at Urbana-Champaign, Urbana, Illinois 61801, United States

Supporting Information

ABSTRACT: The recently emerged selective lateral epitaxy of semiconductor planar nanowires (NWs) via the vapor−liquid−solid (VLS) mechanism has redefined the long-standing symbolic image of VLS NW growth. The in-plane geometry and self-aligned nature make these planar NWs completely compatible with large scale manufacturing of NW-based integrated nanoelectronics. Here, we report on the realization of perfectly site-controlled growth of GaAs planar NW arrays with unity yield using lithographically defined gold (Au) seed dots. The growth rate of the planar NWs is found to decrease with the NW width at fixed spacing, which is consistent with the conventional VLS model based on the Gibbs-Thomson effect. It is found that in general, the planar and out-of-plane NW growth modes are both present. The yield of planar NWs decreases as their lateral dimension shrinks, and 100% yield of planar NWs can be achieved at moderate V/III ratios. Based on a study of the shape of seed particles, it is proposed that the adhesion between the liquid-phase seed particle and the substrate surface is important in determining the choice of growth mode. These studies represent advances in the fundamental understanding of the VLS planar NW growth mechanism and in the precise control of the planar NW site, density, width, and length for practical applications. In addition, high quality planar InAs NWs on GaAs (100) substrates is realized, verifying that the planar VLS growth mode can be extended to heteroepitaxy.

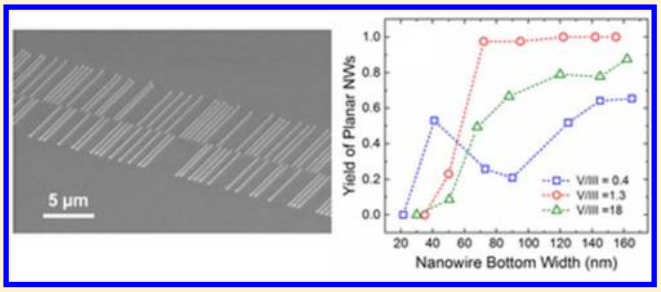

KEYWORDS: *Vapor−Liquid−Solid Mechanism, Planar Nanowire, MOCVD, GaAs, InAs*

Semiconductor nanowires (NWs) hold extreme promises to be the building blocks of future electronics and photonics and, thus, have received tremendous attention for many years.[1−7] Among all kinds of fabrication methods, the bottom-up vapor−liquid−solid (VLS) growth method,[8] where a metallic (e.g., Au) seed particle is used to gather materials and guide NW growth, attracts particular interests owing to its advantages in size downscaling, versatility in the incorporation of doping and heterostrutures,[9−12] and potential in heterogeneous NW integration on foreign substrate[13−17] (for example, III−V NWs on silicon). Ever since the VLS method was invented,[8] NWs standing on substrates and pointing out along surface normal directions have served as the symbolic picture of this method. For III−V materials, these out-of-plane NWs mostly grow along ⟨111⟩B direction.[18] The out-of-plane geometry is not compatible with the well-established planar processing technologies for field-effect transistors (FETs) and, therefore, requires additional processing efforts for device integration. More importantly, the vertical channel structure tends to incur more parasitic capacitance, which degrades the frequency performance (speed) of the device. So far, vertical NW FETs have not shown advantages in speed in comparison to the planar thin-film FETs given the same channel material.[19−21] In this light, selective lateral epitaxy (SLE) of planar NW growth method,[22,23] where NWs are grown out of Au seed particles, via the VLS mechanism, propagating laterally along certain in-plane directions in a self-aligned fashion, has recently emerged. This growth method has not only enriched the fundamental VLS study but also provided a practically useful technology for realizing NW-based integrated circuits. So far, high-performance MESFETs, HEMTs, and MOSFETs devices have been demonstrated using planar NWs as the current conducting channels.[24−27] Circuits have also been demonstrated by interconnecting aligned planar NW MESFET devices.[28] To advance the fundamental VLS study and to better assess the technological potential, a systematic growth study is needed. For doing so, we have first developed array-based GaAs planar NW growth using electron beam lithography (EBL) to predefine the Au seed dots.

Figure 1a and b show representative scanning electron microscope (SEM) images of a GaAs planar NW array grown on a GaAs (100) substrate. The patterned Au dot array was placed at a horizontal line as indicated by red arrows. The center to center spacing between the NWs is 1 μm. The sample shown here was grown in a metal−organic chemical vapor deposition (MOCVD) system under 950 mbar at temperature

Received: July 5, 2014
Revised: October 8, 2014
Published: October 24, 2014

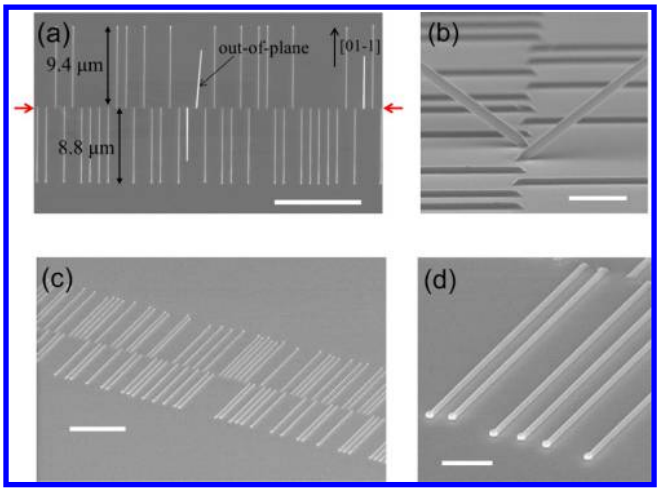

Figure 1. SEM images of GaAs planar NW arrays grown on GaAs (100) substrates. (a) Top-view SEM image of a representative GaAs planar NW array on a (100) substrate. The red arrow indicates where the line of Au dots was initially patterned. Planar NWs were formed as the Au dots propagated upward ([0 1 −1] direction) or downward ([0 −1 1]) during the growth. The three brighter NWs are out-of-plane as indicated. The NW bottom width (trapezoidal cross-section) of this particular array is 145 nm. (b) An 80° tilted-view SEM image of the same sample in (a) clearly showing two out-of-plane NWs. (c) A 60° tilted view of a planar NW array with perfect yield of planar NWs achieved by optimizing the growth condition (see text for details). (d) Higher magnification view of the same array in (c). The Au catalyst dots, which propagated from the center line to guide the NW growth, are clearly visible at the tips of those NWs. The scale bars are 10, 1, 5, and 1 μm for (a)−(d), respectively.

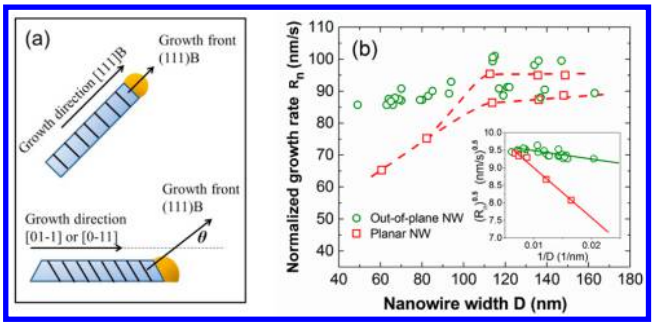

Figure 2. Comparison between growth rates of planar and out-of-plane GaAs NWs. (a) Schematic diagrams of out-of-plane and planar NWs grown on (100) substrate. A normalized growth rate is introduced in the main text for a fair comparison of the two growth modes. (b) Comparison between normalized growth rates of planar NWs and nonplanar NWs. The growth was done at 460 °C with a V/III ratio of 30 under 950 mbar. Each data point (red squares) for planar NWs was measured and averaged from an array with 10 μm spacing. The data for out-of-plane NWs were measured on the same arrays. Each data point (green circles) refers to the growth rate of an individual NW. The dashed lines are only for eye guidance. The inset of (b) shows a linear fit to the square root of growth rate versus the inverse of NW width for both growth modes.

T = 460 °C for 80 s with a nominal V/III ratio of 30. The bidirectional growth[22,29] can be clearly seen in Figure 1a. Interestingly, we observe a noticeable difference in the planar NW lengths and, thus, growth rates between the two presumably crystallographically equivalent directions, with the NWs propagating along [0 1 −1] and the antiparallel [0 −1 1] direction being 9.4 and 8.8 μm in length, respectively. Such a growth rate difference (typically <20%) is only observed on large diameter NWs and disappears when the NW widths are smaller than ∼80 nm. This phenomenon is not the major point here and needs further investigation. We speculate that the preference could be induced by substrate orientation miscut (manufacture specification was ±0.5°), which makes the two directions no longer perfectly equivalent. On this particular sample, a few out-of-plane NWs are observed and can be identified as those brighter (and shorter) NWs in Figure 1a. The out-of-plane NWs grow along ⟨111⟩B directions and, therefore, are aligned at 35.3° with respect to the substrate surface.[22] Figure 1b shows a tilted-view SEM image where two out-of-plane NWs can be clearly seen. Remarkably, the yield of the planar NWs can be improved by tuning the growth conditions (details will be discussed later). Figure 1c and d show exemplary SEM images of the planar NW array with unity yield.

A comparison between the growth rates of planar and out-of-plane NWs is shown in Figure 2. For out-of-plane NWs, the growth direction (direction of facet advancing) and the normal direction of growth front are the same (both ⟨111⟩B),[18] as illustrated by the top schematic in Figure 2a. However, the two directions are different for the planar NW growth. As shown in Figure 2a (bottom schematic), the angle θ between the two directions is 35.3° for planar NW growth on GaAs (100) substrates because the growth direction is either [0 1 −1] or [0 −1 1], whereas the growth front is still (111)B, according to our previous studies.[22,29] Let R_m be the measured NW growth rate, which can be obtained by directly dividing the measured NW length by the growth time. The volume of material deposited per unit area per unit time is $R_m\cos\theta$, where θ is 0° for out-of-plane NWs and 35.3° for planar ones. So, the number of atoms deposited per unit time per unit area is proportional to $R_m\cos\theta$. Therefore, we define a normalized growth rate as $R_n = R_m\cos\theta$ in order to compare the two different types of NWs on an equal footing.

Figure 2b shows the normalized growth rates of planar NWs and out-of-plane NWs measured from the sample prepared under the same growth condition as in Figure 1a. Each of the data points (red squares) for planar NWs was measured and averaged from about 20 NWs in an array with 10 μm spacing between adjacent NWs. The large spacing was designed to minimize any synergetic effect of growth rate between neighboring NWs.[30] Without spacing control in the growth rate study, the real trend can be hidden by density related variations. Five arrays of holes were first patterned on PMMA by EBL with nominal diameters of 300, 250, 200, 150, and 100 nm, respectively. Au dots were then produced by a lift-off process after 30 nm Au film was evaporated. The planar NWs are very uniform in size and growth rate within each array. The standard deviations of growth rate and width are smaller than 3 nm/s and 3 nm, respectively. As seen from Figure 2b, when the NW width is relatively large (>∼ 110 nm in bottom width), two different growth rates are associated with each planar NW size. The growth rate starts to roll off clearly when the width becomes smaller. This is consistent with the conventional VLS model proposed by Givargizov,[31] where smaller NWs are associated with slower growth rates because the NW surface energy reduces supersaturation. The inset of Figure 2b plots the square root of growth rate versus the inverse of NW width (the data points with slower growth rate are adopted for the bimodal cases). A fairly good linear fit can be obtained for planar NWs, supporting the interpretation by the conventional model.[31,32]

dx.doi.org/10.1021/nl502525z | Nano Lett. 2014, 14, 6836−6841

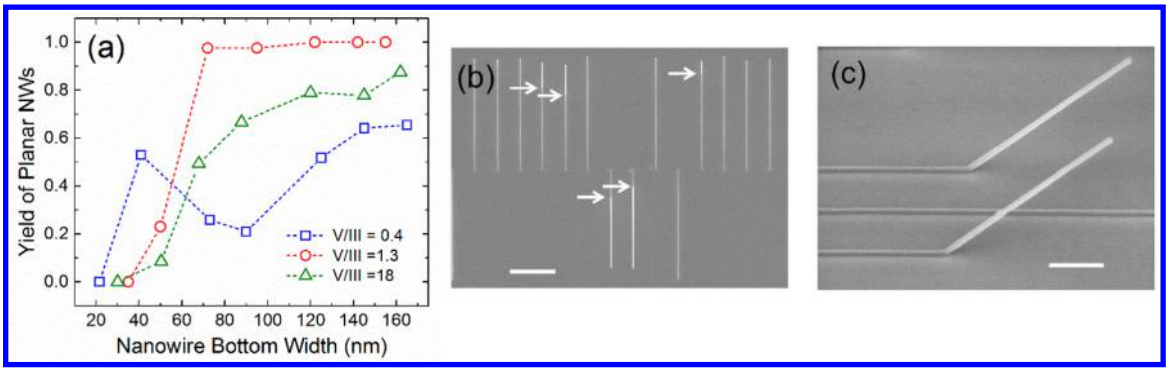

Figure 3. Yield study of VLS GaAs planar NWs. (a) Yield of planar NWs as a function of bottom width. Three samples were prepared with V/III ratios of 0.4, 1.3, and 18, respectively. To vary V/III ratio, we fixed TMGa flow and only the AsH_3 flow was changed across the three samples. Other growth conditions were identical for all the three samples. The growth temperature and reactor pressure were 460 °C and 150 mbar, respectively. (b) Typical SEM image showing the transition regime where some of the planar NWs start to take off from the substrate surface in the middle of the growth. The out-of-plane NWs show brighter contrast in the image. The white arrows indicate the points where the NWs start to take off. The scale bar is 2 μm. (c) A 60° tilted view of the NWs taking off in the middle of the growth. The scale bar is 500 nm.

By extrapolating the fitted line, the critical width is calculated to be ~13 nm for the planar growth.

We were able to measure the length of out-of-plane NWs also from those arrays because the yield of planar NWs was not perfect under that particular growth condition. Note that each of the data points (green circles) of out-of-plane NWs only refers to the growth rate measured from an individual NW. The bimodal rate is also seen for the out-of-plane NWs. The normalized growth rates of planar NWs (slightly slower) match closely with that of out-of-plane NWs, both of which remain a near constant value. This can be understood by the fact that the Gibbs–Thomson effect[31] (NW sidewall energy) is weak for thick NWs and, thus, out-of-plane and planar NWs should have very similar supersaturation, $\Delta\mu$, defined as the difference between chemical potentials of NW materials in the vapor phase and in the NW.[31] As the NW width shrinks down, the growth rate of planar NWs decreases steeper than that of out-plane NWs. Note that this trend, where the two modes have close growth rates at large sizes but planar NWs grow slower at smaller sizes, is true for all growth conditions we have tested. This implies that for smaller sizes, out-of-plane growth is associated with higher supersaturation. In the discussion above, we assume the kinetic parameters that connect supersaturation to growth rate are the same for both types of growth. Though it is open for discussion, this is a reasonable assumption because both planar and out-of-plane NWs are seeded by Au and have (111)B growth fronts. Because they are located on the same sample, they also had experienced exactly identical growth conditions. Another factor that needs to be considered is the surface adatom diffusion, which can affect the NW growth rate and cannot be captured by the conventional model.[33] We have confirmed that the NW growth rate induced by surface diffusion is negligibly small in our experiments (below 1 nm/s, see Supporting Information for the calculation). Note that our observation here is different from an insightful previous study on InAs planar NWs,[34] where it was shown that planar growth was associated with larger supersaturation (less suffered from Gibbs–Thomson effect) due to the removal of substrate surface by planar growth. The contradiction is worth further study, and we speculate that under our growth conditions, the top (100) and sidewall (111)A surface energy of the planar NW is large and makes the overall supersaturation of planar growth smaller despite the removal of the bottom surface.

Figure 3a shows the yield of planar NWs as a function of the NW size (bottom width). The yield here is defined as the ratio between the number of NWs that remain planar throughout the entire growth period and the total number of NWs (81) grown in the array. Three samples grown with different nominal V/III molar flow ratios (0.4, 1.3 and 18) are shown in Figure 3a. To vary V/III ratios, the TMGa flow was fixed and only the AsH_3 flow was changed across the three samples. Other growth conditions were identical, with growth temperature and reactor pressure being 460 °C and 150 mbar, respectively. Multiple Au dot arrays with the same dot size within each array were patterned on each of those samples. The growth rates of large NWs (>120 nm in width) on the samples with V/III ratios of 18, 1.3, and 0.4 are 135, 120, and 40 nm/s, respectively. The corresponding growth times are 50, 50, and 80 s, respectively. For smaller NWs, the growth rate decreases following a similar trend as shown in Figure 2b. From Figure 3a, it can be seen that for NWs with bottom width larger than ~70 nm, the sample with V/III = 1.3 has unity yield of planar NWs. The yields from the other two samples are noticeably lower. In this size range, unity yield can be reproducibly achieved when the V/III ratio ranges from ~0.8 to ~5.

As the NW width becomes smaller, the yield at the optimum V/III ratio of 1.3 drops below 100%, and when the width becomes less than ~50 nm, no planar NWs can be observed. The widths shown in Figure 3a for the zero yield case were measured on out-of-plane NWs. Shown in Figure 3b is a typical SEM image of the transition regime where the planar NW yield has degraded. It is observed that many NWs start the growth in the planar mode but take off from the substrate surface at some point, as indicated by the white arrows in Figure 3b, during the growth. This can be seen more clearly from Figure 3c. The result suggests the presence of a delicate balance between the planar and out-of-plane mode. The other two samples show a similar trend in general, where smaller NWs have lower yield and no planar NWs can be found when the size drops below certain points. A hump at 40 nm NW width is observed on the yield-size curve with V/III = 0.4, which is not understood at this point and needs further study. It has to be mentioned that the cessation of planar NW growth at very small sizes is not because of a complete loss of supersaturation due to the Gibbs–Thomson effect. Extremely high growth rates (~100 nm/s) for planar NWs are still observed from the very low-yield array of small-size NWs. In other words, there still exists a large

dx.doi.org/10.1021/nl502525z | Nano Lett. 2014, 14, 6836–6841

level of supersaturation to support fast planar NW growth. Other underlying reasons that control the preference between planar and nonplanar growth must be considered.

Shown in Figure 4 are two SEM images of Au seeds after growth, where 4a and b show the samples that were cooled

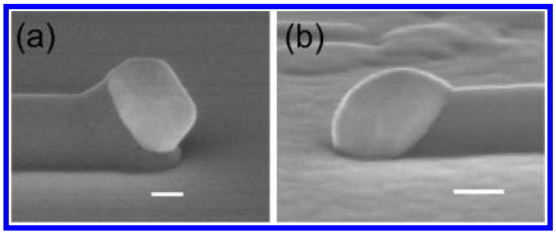

Figure 4. SEM images showing the shapes of seed particles after sample cooling. (a) Cooling with AsH_3 overpressure. (b) Cooling without AsH_3 overpressure. The sample is tilted by 80°. The scale bars are both 100 nm.

down from the growth temperature with and without AsH_3 overpressure, respectively. It is observed that the Au particle in Figure 4a shows a nonspherical shape and a neck-like structure is formed and clearly visible below the Au nanoparticle. This is because with the supply of As precursor during sample cooling, the Ga atoms in the seed particle can continue to precipitate out to form an additional growth segment of GaAs, as is the case for out-of-plane NWs.[35] However, the Au particle in Figure 4b exhibits a rounder profile and only negligible extraneous material is visible below the gold. In the absence of AsH_3 supply, only a very small amount of GaAs can be formed during the cooling process because of the extremely low solubility of As in Au, so the shape of catalyst can be well preserved. Therefore, Figure 4b should more closely represent the actual growth-phase geometry of Au nanoparticles. Importantly, the base of the nanoparticle is in contact with the substrate, which suggests that it was in direct contact with (wetted) the substrate, in addition to the NW growth front, during planar NW growth. Note that in the growth of in-plane InAs NWs, such an additional contact interface was also observed.[23,34]

Based on the experimental analysis above, we propose that the wetting nature of seed droplet on the substrate during growth is an important factor responsible for the planar type of VLS GaAs NW growth. Once the liquid-form seed particle contacts the substrate surface, it needs to overcome the adhesion energy between the seed and the substrate surface before the out-of-plane mode may proceed. Note that it was suggested, in the case of in-plane InAs traces growth on (111)B GaAs,[23] that the Au catalyst stays on the substrate because Au/GaAs interfacial energy is lower than that of Au/InAs interface. We believe that in general, this energy difference is not necessary for the occurrence of planar VLS NW growth because in our case, the Au/GaAs (111)B interface at the growth front should have a lower interfacial energy.[18] We speculate that the wetting was initiated during the oxide desorption procedure at the very beginning of the growth—the gold dots collect materials from the substrate and become eutectic droplets. After the growth precursors are introduced, the planar growth proceeds with materials stacking in a layer-by-layer manner on (111)B facets while the droplet remains in contact with the (100) substrate since (100) is not the growth front. As discussed in refs 36 and 37, perturbations that occur during NW growth might strongly affect the choice of growth modes. Perturbations such as organic residue on the substrate or the occurrence of a stacking fault may interrupt the contact between the seed particle and the substrate and make the NWs switch to the out-of-plane mode. Supporting evidence can be found in our previous study, where the intentional introduction of twinning defects by dopant incorporation caused the planar NW to switch to the out-of-plane growth mode.[38] This explains the fact that even the yield for wide planar NWs is not always perfect except for under optimized V/III ratios. As reported in the recent research on *in situ* TEM observation of III−V VLS NW growth,[39] a growth condition with very high V/III ratio can induce twinning defects, which is likely to disturb the planar growth in our case. The factors discussed above also provide a natural explanation for the size-dependent yield study. Small-size seeds would have less contact area with the substrate so one would expect that it is easier to separate them from the substrate. In other words, the growth of narrower planar NWs should be more vulnerable to perturbations and, thus, shows lower yield. The analysis here implies that the planar type of growth could be universally achievable in any material system if (i) the growth front is not in parallel with the substrate surface and (ii) the adhesion between the substrate and the catalyst can be appropriately engineered.

As an example, we demonstrate here that planar III−V NW growth can be extended to the heteroepitaxy of self-aligned and high-quality InAs on GaAs (100) substrates through the same VLS approach defined above. Growth of planar InAs NWs on a semi-insulating substrate can be a very competitive platform technology for future low-power logic applications given the extremely high electron mobility in InAs. Despite the approximately 6.7% bulk lattice-mismatch, directly interfaced and single-crystalline lateral growth of InAs NWs is realized under optimized growth conditions, with NWs being self-aligned along the ⟨011⟩ direction on GaAs (100) substrates. Note that the ⟨011⟩ direction observed here is orthogonal to the ⟨0-11⟩ directions towards which planar GaAs NWs on GaAs (100) and planar InAs NWs on InAs (100) substrates are oriented.[34,40] This difference will be explored in a future study. Figure 5a shows a tilted-view SEM image of two as-grown InAs NWs on GaAs (100). We note that Au-seed particles are clearly identified at the NW tips, characteristic of VLS-type growth, while the NW widths exhibits no structural variations (twinning or tapering) along their lengths. Figure 5b shows a cross-sectional view high-resolution transmission electron microscopy (HR-TEM) image of a laterally grown InAs NW on GaAs. The NW body and GaAs substrate share an atomically abrupt interfacial plane (dashed line, Figure 5b), with the NW assuming the same zinc-blende structure as the substrate. The Au seed appears raised relative to the substrate surface, likely resulting from post growth-termination precipitation of growth species from the liquid-phase alloy in an AsH_3-rich environment, as is the case for planar GaAs NWs. Analytic-TEM characterization (refer to Supporting Information) confirms the Hetero-SLE NW crystal quality (no stacking faults) and composition.

In summary, we have performed a systematic experimental study of the VLS growth of GaAs planar NWs from various aspects. The size-dependent growth rate and yield of planar NWs have been studied. Careful control of growth conditions can lead to unity yield of planar NWs. We have also shown that the liquid-phase seed particle contacts the substrate surface during growth and have proposed that the adhesion energy is important in determining the choice of growth mode. We

dx.doi.org/10.1021/nl502525z | *Nano Lett.* 2014, 14, 6836−6841

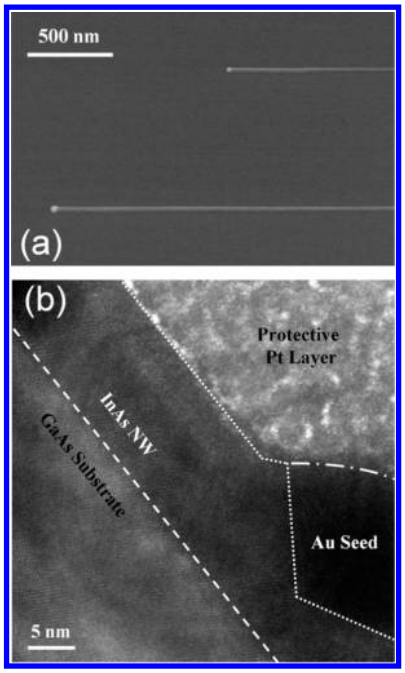

Figure 5. Heteroepitaxial VLS InAs planar NWs on semi-insulating GaAs (100). (a) Tilted-view SEM image showing parallel growth of two planar InAs NWs on a GaAs substrate. (b) Cross-sectional HR-TEM image of a ∼12 nm-thick planar InAs NW directly interfaced with the underlying GaAs substrate.

believe that the well-controlled planar type of VLS growth can be extended beyond the scope of homoepitaxy and it is demonstrated by the growth of high-quality (free of stacking faults) InAs planar NWs on GaAs (100) substrates.

Methods. *Planar NW Growth.* To grow GaAs planar NW arrays, we first defined Au seed particles on GaAs (100) substrates by electron beam lithography patterning (with a Raith e-line system) and electron beam evaporation of Au. The samples then went through an intensive cleaning procedure to ensure the removal of organic residues. The samples were then loaded into an Aixtron 200 atmospheric pressure MOCVD reactor, followed by an oxide desorption step at 680 °C. The temperature was then lowered to 460 °C and GaAs NW arrays were grown by using AsH_3 and Trimethyl-gallium (TMGa) as As and Ga precursors, respectively. The planar InAs NW growth was carried out in the same reactor. Au nanoparticles (5 nm in diameter) were randomly dispersed on the GaAs (100) substrate from the commercial Au colloidal solution (BBInternational, U.K.). After an oxide desorption step at 625 °C, InAs planar NWs were then grown at 360 °C with AsH_3 and trimethylindium (TMIn) as precursors.

Characterization. The GaAs planar NW samples were inspected by a Hitachi S4800 SEM instrument. The nanowire length and bottom width were determined by the same SEM instrument. A JEOL 2010F system was employed for all scanning transmission electron microscopy (STEM) experiments. Single NW TEM lamellae were prepared using an FEI Helios NanoLab 600i focused ion-beam (FIB) system.

■ ASSOCIATED CONTENT

Ⓢ Supporting Information

An estimation of growth rate contributed from surface diffusion; A HR-TEM image obtained at the InAs NW/GaAs substrate interface and corresponding FFT pattern; a HAADF-STEM image showing the tip of a heteroepitaxial, planar InAs NW; a figure showing EDXS line-scan results from the GaAs substrate to the NW body then to the Au seed particle, which confirms the chemical composition of the InAs NW. This material is available free of charge via the Internet at http://pubs.acs.org.

■ AUTHOR INFORMATION

Corresponding Author

* E-mail: xiuling@illinois.edu.

Notes

The authors declare no competing financial interest.

■ ACKNOWLEDGMENTS

We are grateful for the support from the Division of Materials Research (DMR) from NSF under grant #1006581. Materials growth experiments were carried out in the Micro and Nanotechnology Laboratory, University of Illinois. P.K.M. gratefully acknowledges FIB assistance from Dr. Jim Mabon. Materials characterization experiments were carried out in part in the Frederick Seitz Materials Research Laboratory Central Research Facilities, University of Illinois.

■ REFERENCES

(1) Cui, Y.; Lieber, C. M. *Science* **2001**, *291*, 851−853.
(2) Duan, X.; Huang, Y.; Agarwal, R.; Lieber, C. *Nature* **2003**, *421*, 241−245.
(3) Xu, S.; Qin, Y.; Xu, C.; Wei, Y.; Yang, R.; Wang, Z. L. *Nat. Nanotechnol.* **2010**, *5*, 366−373.
(4) Takei, K.; Takahashi, T.; Ho, J. C.; Ko, H.; Gillies, A. G.; Leu, P. W.; Fearing, R. S.; Javey, A. *Nat. Mater.* **2010**, *9*, 821−826.
(5) Tomioka, K.; Yoshimura, M.; Fukui, T. *Nature* **2012**, *488*, 189−192.
(6) Bertness, K. A.; Sanford, N. A.; Davydov, A. V. *IEEE J. Sel. Topics Quantum Electron.* **2011**, *17*, 847−858.
(7) Nguyen, H. P. T.; Zhang, S.; Cui, K.; Han, X.; Fathololoumi, S.; Couillard, M.; Botton, G. a; Mi, Z. *Nano Lett.* **2011**, *11*, 1919−1924.
(8) Wagner, R. S.; Ellis, W. C. *Appl. Phys. Lett.* **1964**, *4*, 89−90.
(9) Perea, D. E.; Hemesath, E. R.; Schwalbach, E. J.; Lensch-Falk, J. L.; Voorhees, P. W.; Lauhon, L. J. *Nat. Nanotechnol.* **2009**, *4*, 315−319.
(10) Tian, B.; Zheng, X.; Kempa, T. J.; Fang, Y.; Yu, N.; Yu, G.; Huang, J.; Lieber, C. M. *Nature* **2007**, *449*, 885−889.
(11) Lind, E.; Persson, A. I.; Samuelson, L.; Wernersson, L.-E. *Nano Lett.* **2006**, *6*, 1842−1846.
(12) Qian, F.; Li, Y.; Gradecak, S.; Wang, D.; Barrelet, C. J.; Lieber, C. M. *Nano Lett.* **2004**, *4*, 1975−1979.
(13) Mårtensson, T.; Svensson, C. P. T.; Wacaser, B. A.; Larsson, M. W.; Seifert, W.; Deppert, K.; Gustafsson, A.; Wallenberg, L. R.; Samuelson, L. *Nano Lett.* **2004**, *4*, 1987−1990.
(14) Davydok, A.; Breuer, S.; Biermanns, A.; Geelhaar, L.; Pietsch, U. *Nanoscale Res. Lett.* **2012**, *7*, 109.
(15) Mazid Munshi, M.; Dheeraj, D. L.; Fauske, V. T.; Kim, D.-C.; van Helvoort, A. T. J.; Fimland, B.-O.; Weman, H. *Nano Lett.* **2012**, *12*, 4570−4576.
(16) Woodruff, J. H.; Ratchford, J. B.; Goldthorpe, I. a; McIntyre, P. C.; Chidsey, C. E. D. *Nano Lett.* **2007**, *7*, 1637−1642.
(17) Mohseni, P.; Behnam, A.; Wood, J.; English, C. D.; Lyding, J. W.; Pop, E.; Li, X. *Nano Lett.* **2013**, *13*, 1153−1161.
(18) Fortuna, S. A.; Li, X. *Semicond. Sci. Technol.* **2010**, *25*, 024005.
(19) Egard, M.; Johansson, S.; Johansson, a. C.; Persson, K. M.; Dey, a. W.; Borg, B. M.; Thelander, C.; Wernersson, L. E.; Lind, E. *Nano Lett.* **2010**, *10*, 809−812.
(20) Johansson, S.; Memisevic, E.; Wernersson, L.-E.; Lind, E. *IEEE Electron Device Lett.* **2014**, *35*, 518−520.
(21) Kim, D.; del Alamo, J. *IEEE Electron Device Lett.* **2010**, *31*, 806−808.

(22) Fortuna, S. A.; Wen, J.; Chun, I. S.; Li, X. *Nano Lett.* **2008**, *8*, 4421−4427.
(23) Zhang, X.; Zou, J.; Paladugu, M.; Guo, Y.; Wang, Y.; Kim, Y.; Joyce, H. J.; Gao, Q.; Tan, H. H.; Jagadish, C. *Small* **2009**, *5*, 366−369.
(24) Fortuna, S.; Li, X. *IEEE Electron Device Lett.* **2009**, *30*, 593−595.
(25) Dowdy, R.; Walko, D. A.; Fortuna, S. A.; Li, X. *IEEE Electron Device Lett.* **2012**, *33*, 522−524.
(26) Miao, X.; Zhang, C.; Li, X. *Nano Lett.* **2013**, *13*, 2548−2552.
(27) Zhang, C.; Li, X. *Solid-State Electron.* **2014**, *93*, 40−42.
(28) Zhang, C.; Dowdy, R.; Li, X. *Device Research Conference (DRC)* **2013**, 63−64.
(29) Dowdy, R.; Walko, D.; Li, X. *Nanotechnology* **2013**, *24*, 035304.
(30) Borgström, M. T.; Immink, G.; Ketelaars, B.; Algra, R.; Bakkers, E. P. a M. *Nat. Nanotechnol.* **2007**, *2*, 541−544.
(31) Givargizov, E. *J. Cryst. Growth* **1975**, *31*, 20−30.
(32) Dayeh, S. A.; Picraux, S. T. *Nano Lett.* **2010**, *10*, 4032−4039.
(33) Fröberg, L.; Seifert, W.; Johansson, J. *Phys. Rev. B* **2007**, *76*, 153401.
(34) Zi, Y.; Jung, K.; Zakharov, D.; Yang, C. *Nano Lett.* **2013**, *13*, 2786−2791.
(35) Persson, A. I.; Larsson, M. W.; Stenström, S.; Ohlsson, B. J.; Samuelson, L.; Wallenberg, L. R. *Nat. Mater.* **2004**, *3*, 677−681.
(36) Schwarz, K. W.; Tersoff, J. *Nano Lett.* **2011**, *11*, 316−320.
(37) Schwarz, K. W.; Tersoff, J. *Nano Lett.* **2012**, *12*, 1329−1332.
(38) Dowdy, R. S.; Zhang, C.; Mohseni, P. K.; Fortuna, S. A.; Wen, J.-G.; Coleman, J. J.; Li, X. *Opt. Mater. Express* **2013**, *3*, 1687.
(39) Chou, Y.-C.; Hillerich, K.; Tersoff, J.; Reuter, M. C.; Dick, K. a; Ross, F. M. *Science* **2014**, *343*, 281−284.
(40) Jung, K.; Mohseni, P. K.; Li, X. *Nanoscale* **2014**, DOI: 10.1039/C4NR04670F.